Characterizing most irregular small scale structures in turbulence using local Hölder exponents

Florian Nguyen, Jean-Philippe Laval, Bérengère Dubrulle

Characterizing most irregular small scale structures in turbulence using local Hölder exponents

F. Nguyen[1], J-P. Laval[1], B. Dubrulle[2]

[1]Univ. Lille, CNRS, ONERA, Arts et Metiers Institute of Technology, Centrale Lille, UMR 9014 - LMFL - Laboratoire de Mécanique des fluides de Lille - Kampé de Fériet, F-59000 Lille, France

[2]Universite Paris-Saclay, CNRS,CEA, SPEC, F-91190 Gif sur Yvette Cedex, France

(Received xx; revised xx; accepted xx)

Two scalar fields characterizing respectively pseudo-Holder exponents and local energy transfers are used to capture the topology and the dynamics of the velocity fields in areas of lesser regularity. The present analysis is conducted using velocity fields from two Direct Numerical Simulations (DNS) of the Navier-Stokes equations in a triply periodic domain. A "typical irregular structure" is obtained by averaging over 200 most irregular events. Such structure is similar to a Burgers vortex, with small non-axisymmetric corrections. A possible explanation of such asymmetry is provided by a detailed time-resolved analysis of birth and death of the irregular structures, which shows that they are connected to vortex interactions, possibly vortex reconnection.

1. Introduction.

Batchelor & Townsend (1949) speculated about the nature of small scale turbulent motions on the basis of hot wire velocity measurements in the Cavendish wind tunnel. Their main conclusion was that the energy associated with small scales is intermittent in space and time and organized into strong discrete vortices. Since then, progresses in computer power and image velocimetry has made it possible to investigate in more detail the nature and the properties of small scale turbulent motions, at scales of the order of or below the Kolmogorov scale. For example, it is now well established that regions where the vorticity supersedes the strain (the so-called Q criterion) are indeed organized into small scale elongated coherent structures that display a complex dynamics (e.g. Vincent & Meneguzzi 1994). In some circumstances, they may interact and reconnect iteratively, following a self-similar vortex reconnection cascade. During reconnection, a distinct $-5/3$ inertial range is observed for the kinetic energy spectrum, associated with numerous resulting fine-scale bridgelets and thread filaments (e.g. Yao & Hussain 2020).

In the mean time, theoretical models of vortex reconnection using Biot-Savart model have evidenced a self-similar process, resulting in a near finite time singularity at the apex of the tent formed by the vortices (Kimura & Moffatt 2014). Another evidence for quasi blow-up is provided by the "zeroth law of turbulence" (see Frisch 1995), according to which the non-dimensional energy per unit mass becomes constant at large Reynolds number, implying a blow up of the enstrophy in the limit of zero viscosity. This suggests that the small scale structure of turbulent motions is very irregular, and calls for specific tools to analyze them. A suitable tool to deal with them was invented by Leray (1934) and named "weak formulation". The main idea is to make a detour via the scale space, and work with a coarse version of the initial field (a "mollified" field), over a characteristic

scale (resolution) ℓ. At any given resolution ℓ, the mollified field is sufficiently regular, so that all classical tools and manipulation of analysis of vector fields are valid. Limiting behaviors as resolution $\ell \to 0$ can then be used to infer results and properties for the rough field.

In previous work, we showed how these vector fields can be used to build two scalar fields, that encode the regularity properties of the small scale motions: i) a pseudo-Holder exponent $\tilde{h}(\mathbf{x})$ built using the *Wavelet Transform Modulus Maxima* (WTMM) method and providing the best local estimate of Hölder regularity compatible with the global multi-fractal analysis (see Nguyen et al. 2019); ii) a local energy transfer $D^I_\ell(\mathbf{x})$ built using the energy balance of the weak solutions to Navier–Stokes equations (Kuzzay et al. 2017; Dubrulle 2019).

In the present paper, we apply these tools to velocity fields issued from Direct Numerical Simulations (DNS) of the Navier-Stokes equations in a triply periodic domain, to capture the topology and the dynamics of the velocity fields in areas of lesser regularity. We further compute a "typical irregular structure" by averaging over 200 most irregular events. Such typical structure is similar to a Burgers vortex, with small non-axisymmetric corrections. A possible explanation of such asymmetry is provided by a detailed time-resolved analysis of birth and death of the events, which shows that they are connected to vortex interactions, possibly vortex reconnections.

2. Tools for studying irregular motions

In order to probe areas of lesser regularity in the flow, we use two different tools, based upon weak formulation. The first one is based on velocity increments computed using weak derivatives of the velocity field and quantifies its local regularity, while the second is based upon weak divergence of the cube of the velocity increment, and characterizes energy transfers across scales.

2.1. *The local Hölder exponents.*

To quantify the regularity of the field, we use the concept of Hölder continuity. A velocity field is said to be h-Hölder continuous with some exponent $h < 1$ if there exists C such that for ℓ small enough:

$$|\boldsymbol{u}(\mathbf{x}+\boldsymbol{\ell}) - \boldsymbol{u}(\mathbf{x})| < C\ell^h. \tag{2.1}$$

where $\boldsymbol{u}(\boldsymbol{x})$ is the velocity field.

This regularity condition is intermediate between simple continuity and differentiability and is based on the velocity increment $\delta\mathbf{u}(\mathbf{x},\boldsymbol{\ell}) = \mathbf{u}(\mathbf{x}+\boldsymbol{\ell}) - \mathbf{u}(\mathbf{x})$.

We have developed a method to compute an estimate of the local Hölder exponent $\tilde{h}(\boldsymbol{x})$ using a local statistical method (see Nguyen et al. 2019). The scalar field computed using this method is continuous in space and shares the properties of the true Hölder exponent. In particular, the value of $\tilde{h}$ gets lower for areas of lesser local regularity, which makes it a good criterion to detect irregular events.

The method first involves measuring two statistical quantities. The first one is the multifractal spectrum $C(h)$ obtained using the WTMM method (see Kestener & Arneodo 2004). This corresponds to the rate function of the Hölder exponent, obtained in the $\ell \to 0$ limit as

$$\mathrm{Prob}\left[\ln(\delta\boldsymbol{u}) = h\ln(\ell/L)\right] \sim e^{\ln(\ell/L)C(h)} = \left(\frac{\ell}{L}\right)^{C(h)}. \tag{2.2}$$

In the multifractal interpretation of Parisi & Frisch (1985), the quantity $D(h) = 3 - C(h)$

corresponds to the fractal dimension of the sub-space of Hölder exponent h. The multifractal spectrum is connected with the scaling exponents of the velocity structure function through a Legendre transform property: $\zeta(p) = \min_h(ph + C(h))$, where $\langle \big(\delta\mathbf{u}(\mathbf{x}, \boldsymbol{\ell})\big)^p \rangle \sim \ell^{\zeta(p)}$.

The second statistical quantity is the fractal dimension of the boundaries of active volumes as defined by Nguyen et al. (2019). These volumes characterize regions of large velocity gradients in a turbulent vector field. An active volume A_p is defined by:

$$\mathbf{x} \in A_p \quad iff \quad \|\delta\mathbf{u}(\mathbf{x}, \boldsymbol{\ell})\| \geqslant c_p \mathcal{S}_p(\ell), \tag{2.3}$$

where c_p is a scale independent constant and $\mathcal{S}_p(\ell)$ is a threshold defined by:

$$\mathcal{S}_p(\ell) = \exp\left(\frac{\langle \ln\big(\delta\mathbf{u}(\mathbf{x}, \boldsymbol{\ell})\big) \big(\delta\mathbf{u}(\mathbf{x}, \boldsymbol{\ell})\big)^p \rangle}{\langle \big(\delta\mathbf{u}(\mathbf{x}, \boldsymbol{\ell})\big)^p \rangle} \right). \tag{2.4}$$

From its definition, it can be shown that such threshold obeys the scaling law $\mathcal{S}_p(\ell) \propto \ell^{h(p)}$, with $h(p) = d\zeta(p)/dp$, which makes the definition of active volumes parallel to the property of Hölder exponents from (2.1). This leads us to interprete the boundaries of active volumes as sets corresponding to a given local Hölder exponent. The fractal dimension of those boundaries can be measured using a box counting method.

The core of the method thus consists in matching the box counting dimensions from the active volumes to the multifractal spectrum:

$$h_\ell(p) = f_\ell(c_p \mathcal{S}_p(\ell)). \tag{2.5}$$

This results in a direct correspondence from the velocity increments to the local Hölder exponents:

$$\tilde{h}_\ell(\boldsymbol{x}) = f_\ell(\|\delta\mathbf{u}(\mathbf{x}, \boldsymbol{\ell})\|). \tag{2.6}$$

This matching also provides a value for the coefficients c_p. Since these coefficients are scale independent, they can be computed at one scale (e.g. in the inertial range, where scaling laws extend over a wide interval) once and for all, and then be used at any other scale to determine the function f_ℓ. The ℓ subscript denotes a dependency of the Hölder exponent that we compute with respect to scale. Indeed, due to viscous effects, the velocity field becomes more and more regular as ℓ decreases, i.e. $\tilde{h}_\ell(\boldsymbol{x})$ increases. At some locations where the velocity field is irregular, however, such exponent may conserve a value of $\tilde{h}_\ell(\boldsymbol{x}) < 1$, even when we reach the dissipative range. The tracking of very irregular areas will then be done by monitoring the lowest values of $\tilde{h}_\ell(\boldsymbol{x})$, at the Kolmogorov scale $\ell = \eta$.

The tilde marks the difference between our estimation and the real Hölder exponents. Indeed, the field $\tilde{h}_\ell(\boldsymbol{x})$ computed using this method is continuous in space, at variance with the standard multifractal picture. Nguyen et al. (2019) nevertheless proved that it behaves like a real Hölder exponent and can be used to detect potential singularities. For simplicity, we omit the subscript and tilde from the local Hölder exponent in the sequel.

2.2. *The Duchon–Robert energy transfer.*

Another indicator of regularity properties of the velocity field is the local transfer of energy across scales. Indeed, a real singularity is expected to carry energy at a scale $\ell \to 0$. As a consequence, we expect that very irregular fields carry energy at scale below the Kolmogorov scale $\ell < \eta$ before it eventually gets dissipated through viscous effects.

This view was formalized by Duchon & Robert (2000). They define local energy

Run	L	λ	η	$\langle u^2\rangle^{1/2}$	ϵ	ηk_{max}	Re	Re_λ
I	0.79	0.19	0.0083	0.54	0.089	2.1	570	140
II	0.94	0.48	0.034	0.55	0.097	8.5	104	53

TABLE 1. Parameters used in the simulations with resolution 768^3. L is the integral scale, λ is the Taylor scale, η is the Kolmogorov scale, $\langle u^2\rangle^{1/2}$ is the rms velocity, ϵ is the energy dissipation rate, ηk_{max} characterizes the resolution ($\eta k_{max} > \pi$ is well resolved), Re is the Reynolds number based on the integral scale, and Re_λ is the Taylor based Reynolds number.

transfers from large to small scales at scale ℓ using a wavelet transform:

$$D_I^\ell(\boldsymbol{x}) = \frac{1}{4}\int \boldsymbol{\nabla}\Psi^\ell(\boldsymbol{y})\cdot\delta\boldsymbol{u}(\boldsymbol{x},\boldsymbol{y})\|\delta\boldsymbol{u}(\boldsymbol{x},\boldsymbol{y})\|^2\mathrm{d}\boldsymbol{y} \tag{2.7}$$

where $\Psi^\ell(\boldsymbol{x}) = \Psi(\boldsymbol{x}/\ell)/\ell^3$ and Ψ is a regular, even, non negative function with norm 1.

Similarly, one can compute the energy locally dissipated by viscosity by the following (see Dubrulle 2019):

$$D_\nu^\ell = \frac{\nu}{2}\int \boldsymbol{\nabla}^2\Psi^\ell(\boldsymbol{y})\|\delta\boldsymbol{u}(\boldsymbol{x},\boldsymbol{y})\|^2\mathrm{d}\boldsymbol{y}. \tag{2.8}$$

If the velocity is locally Hölder continuous with exponent h, $\delta u \sim \ell^h$, so then $D_I^\ell \sim \ell^{3h-1}$ and $D_\nu^\ell \sim \nu\ell^{2h-2}$. The two terms are balanced at a scale:

$$\eta_h \propto \nu^{1/(h+1)}. \tag{2.9}$$

This corresponds to the classical Kolmogorov scale η for $h = 1/3$, which is the value predicted by Kolmogorov (1941). This also means that the regularizing scale η_h gets lower than Kolmogorov scale if $h < 1/3$. Note that a real singularity occurs with a Hölder coefficient of $h = -1$ since $\eta_{-1} = 0$, so that the velocity field is never regularized.

These estimates show that the regions where the local energy transfer D_I^ℓ stays larger than the dissipation D_ν^ℓ for a scale ℓ close to Kolmogorov scale are very irregular and can be interpreted as quasi singularities. In practice, this corresponds to extreme values of D_I^ℓ.

3. Events in simulations.

In order to search for extreme events at the dissipative scale, we used the two simulations described by Nguyen et al. (2019). For the sake of convenience, the parameters for the simulation are reported in the table 1. Run I has larger Reynolds number, but a small dissipative range. Run II has a smaller Reynolds number, but an extended dissipative range. In the sequel, we use both runs as complementary tools to extract the indicators of irregularity.

3.1. *Calibration of the local Hölder.*

The *WTMM* method is difficult to use in the dissipative range as it requires scaling laws to work over a wide range of scale. As a consequence, the method we use to get the local Hölder exponents requires to compute the c_p coefficients in the inertial range using the Run I. All wavelets transforms are performed using a Mexican wavelet. Indeed, we are probing the dissipative scales were the local Hölder exponent is expected to reach values above 2 (i.e. the velocity field is expected to be at least twice differentiable in most of the space). The first three moments of the Mexican wavelet are null, which allows to measure Hölder exponents up to 3 (see Arneodo et al. 2000).

As our objective is to probe for very singular events, we must increase the range of p compared to our previous work in order to increase the range of velocity increments to

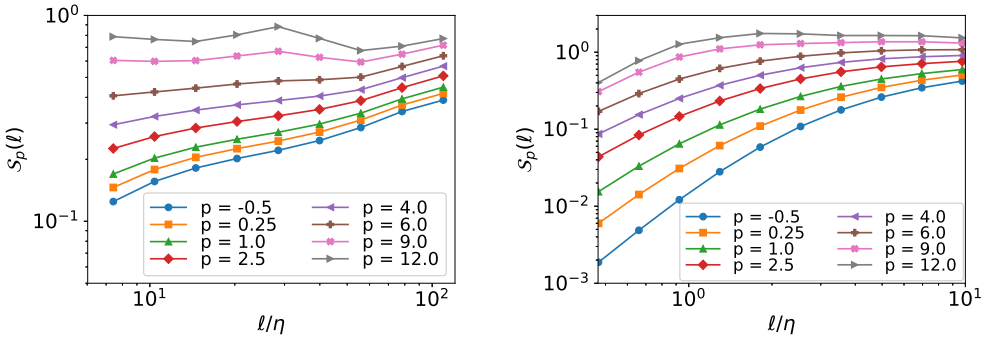

(a) (b)

FIGURE 1. (a) Thresholds $\mathcal{S}_p(\ell)$ for various values of p computed in the inertial range using the velocity fields from Run I. (b) Thresholds $\mathcal{S}_p(\ell)$ for the same p computed in the dissipative range using the velocity fields from Run II.

which we can assign a value of Hölder exponent $\tilde{h}$. The thresholds $S_p(\ell)$ are thus computed with up to $p = 12$ in the vicinity of the inertial range, as shown in figure 1a. One problem with this method is that the convergence is not guaranteed for the highest values of p. We indeed observe that the scaling laws used to determine $h(p)$ in the inertial range for $p \geqslant 9$ are less accurate. As a consequence, the values of local Hölder corresponding to extreme events are subject to approximations. Using the process described in the previous paper, we are able to extract the coefficients c_p by matching the multifractal spectra from the WTMM with the results from boxcounting.

In parallel, we compute the thresholds $S_p(\ell)$ around the dissipative range for the Run II, as well as the power laws $S_p(\ell) \propto \ell^{h(p)}$ as shown in figure 1b. Because the flows are similar and the coefficient c_p do not depend on the scale, we can use the result from the inertial range to compute the mapping function from the velocity increments to the local Hölder exponents at the scale $\ell = 0.06 \approx 2\eta$ using (2.5) and (2.6). This scale is within the dissipative range but large enough such that the wavelets are guaranteed to be well resolved. This also guarantees that we do not reach the limit value of $h = 3$. The mapping function obtained is reported in figure 2. Because the nature of the method giving this mapping function is statistical, we do not expect it to reach the values of velocity increments corresponding to the rarest events. In order to at least give an estimation of the local Hölder exponent in this case, we have to use extrapolation. Furthermore, the values of h given for $\|\delta \boldsymbol{u}\| \geqslant 2$ correspond to order $p \geqslant 10$ which relies on imperfectly converged statistics. We use a conservative extrapolation for higher values of velocity increments, but we can estimate an error on the value of h of the order of 0.2 for h close to 0.

Note that we did not compute an estimate of the local Hölder exponent for very small values of velocity increment. This does not affect our study of very singular events.

3.2. *Statistical study using uncorrelated data.*

The first step to characterize extreme events at the dissipative scale is to get statistics using uncorrelated velocity fields. For that purpose, we use 90 velocity fields of Run II saved over 50 turnover time. On those fields, we compute the local Hölder exponents using the mapping function from figure 2. We then extract all events where the local Hölder exponents get below the threshold value of $h = 0.7$. This value is low enough for

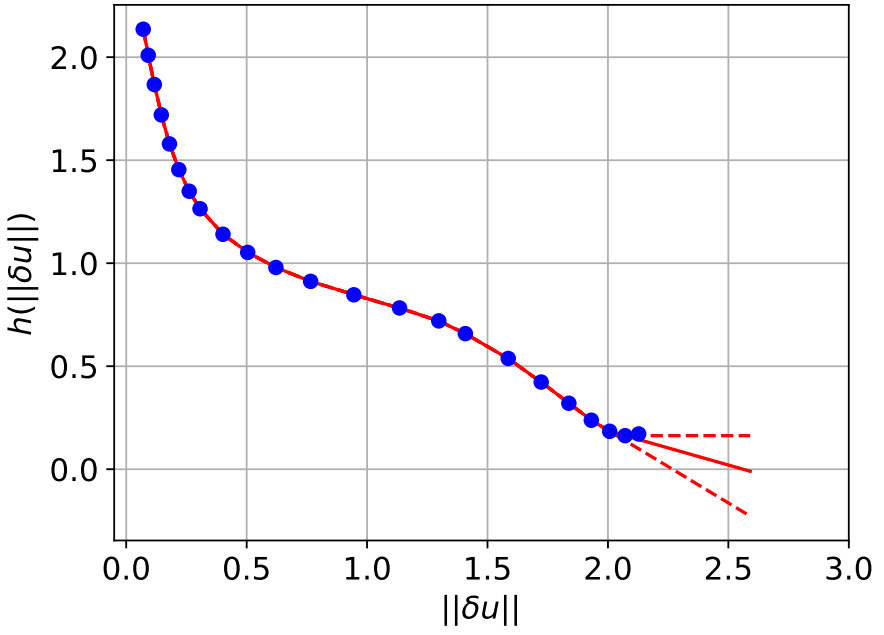

FIGURE 2. Function linking the velocity increment to a value of local Hölder exponent at the scale 2η. The blue dots stands for the values coming directly from the estimation method. The continuous red line corresponds to the function actually used to compute Hölder exponents in the vicinity of quasi singularities. The dotted red lines materialize the uncertainty in the extrapolated part.

the corresponding velocity field to be considered very irregular at the dissipative scale, but high enough to collect an adequate amount of statistics. 470 distinct events fulfilling this condition were detected.

Additionally, we also compute various scalars to help characterizing the corresponding events. Those include the vorticity, the inter scale energy transfer D_I^ℓ and the viscous dissipation at this scale D_ν^ℓ. The invariants of the mollified velocity gradients Q and R are also computed using a Mexican wavelet transform at the same scale for the sake of coherence and comparison with the local Hölder exponent. For an incompressible flow, this leads to:

$$Q = -\frac{1}{2}\,\mathrm{Tr}(A_\ell^2), \tag{3.1}$$

$$R = -\det(A_\ell) \tag{3.2}$$

where:

$$A_{\ell,ij} = -\int \nabla_j G^\ell(\boldsymbol{y}) u_i(\boldsymbol{x}+\boldsymbol{y}) \mathrm{d}\boldsymbol{y}. \tag{3.3}$$

with G^ℓ the mexican wavelet at scale ℓ. Meanwhile, we choose a Gaussian for the function Ψ used for the computations of D_I^ℓ and D_ν^ℓ from (2.7) and (2.8). This would be the equivalent of computing the derivatives with a Gaussian wavelet.

As the events display arbitrary orientation, they are reoriented such that their main

axis is oriented along the x-axis. This axis is determined by the local Hölder exponent using the first eigenvector of the covariance matrix of h. We have checked that such axis also corresponds to the axis along which vorticity lines extend. We also observe in the energy transfer terms that the events are not axisymmetrical around this first axis. This leads us to determine a secondary axis using the orientation of the dissipative pattern of D_ν^ℓ which is oriented along the y-axis in the following figures. Visualizations of physical quantities in a sub-domain of 1.7 cubic Taylor scale around each event are provided in the Supplementary Materials. The events are sorted by minimum value of h, from the most to the least singular. All the figures are made in the reference frame of the structure by removing the mean velocity computed over each sub domain. The figures are composed of visualization of the velocity field and vorticity field in three orthogonal planes intersecting at the most singular point; visualizations of isosurfaces for the vorticity, local Hölder exponent h, local energy transfer D_I^ℓ, and local viscous dissipation D_ν^ℓ; scatter plot of Q and R colored by local Hölder and local energy transfer; and streamlines of velocity.

From the point of view of the Hölder exponent, the most singular event observed reaches a minimum value of $h = \pm 0.2$. We observe a total of 33 events with a Hölder coefficient lower than $1/3$, value under which the regularizing scale η_h from (2.9) gets lower than the Kolmogorov scale η. On one hand, the small number of events considering the amount of statistics used (more than 40 millions data points) is a testimony of their rarity. On the other hand, the inequality $\eta_h < \eta$ means that those are events that might have been under-resolved by the simulation despite the intense energy transfers (more than 100 times the average dissipation rate ϵ).

The extreme values are only reached in a small region. As a result, the choice of the extrapolation of the mapping function in figure 2 has little effect on the results presented below.

A more direct look at those events shows that they all appear to be vortices, with different behaviour of the helicity within the structures. This is confirmed quantitatively by the velocity gradient tensor invariants Q and R. Indeed, the center of the events, defined as the point of minimum local Hölder exponent, is always in the $Q > 0$ regions corresponding to vortices (see Ooi et al. 1999). We do not observe a particular bias toward the vortex stretching or the vortex compressing region in this dataset.

For a large majority of our events, the helicity changes sign over the structure (we call them roll vortices). An example of such event is displayed in figure 3a. Some of them appear off centered as the change of helicity does not happen at the same location as the minimum of Hölder exponent. This might still be the effect of the large scale velocity not being completely removed. In few cases, the helicity does not change sign over the structure (we call them screw vortices). The most singular event where a change of helicity does not appear within the boundaries of the cube extracted is only the 152th most singular (see figure 3b). Meanwhile, we do not observe any qualitative difference in the energy transfer terms or the velocity gradient tensor invariants between roll vortices and screw vortices. This leads us to believe that there is no clear separation between these two categories and that these events share the same mechanism.

In a recent experiment, Debue et al. (2020) also found that extreme events of D_I^ℓ, besides screw and roll vortices, also appear under the shape of "U-turns" characterized by sudden change of direction for the velocity streamlines. In our data, we do not observe any "U-turns". More precisely, while some events look similar to what was found by Debue (see event 107 in Supplementary Materials), a more detailed examination shows that they are actually tighter vortices. A possible explanation for this difference is that

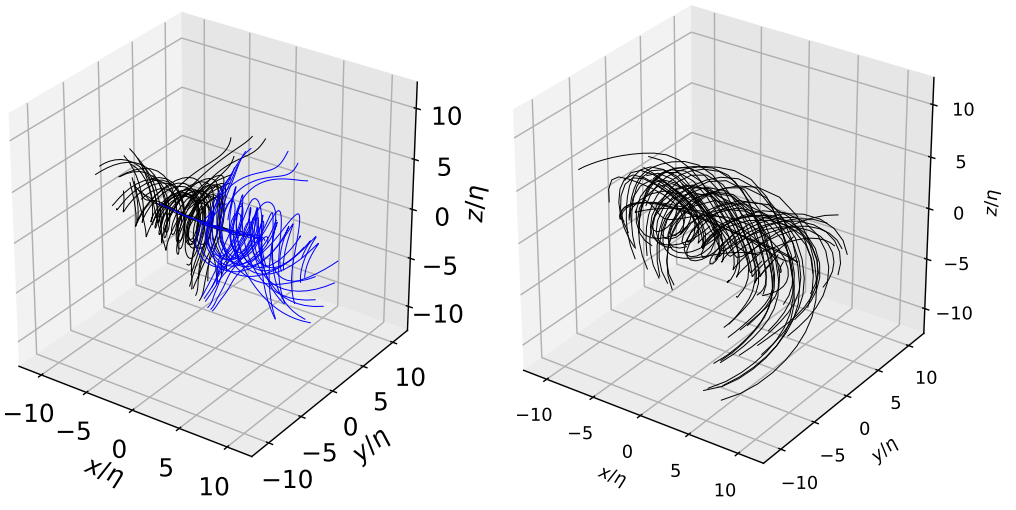

FIGURE 3. (a): Streamlines of velocity for a "roll-vortex" event. Two different colors of streamlines are used to visualize the change of direction: the axial velocity is oriented away from the $x = 0$ plane. This is event 2 from the Supplementary Materials. (b): Streamlines of velocity for a "screw-vortex" event. The axial velocity is oriented toward $x > 0$. This is event 151 from the Supplementary Materials.

we have access to smaller scales compared to Debue et al. (2020), which combined with the absence of experimental noise allows us to better identify the vortices.

3.3. *Typical event*

As we have extracted and reoriented the extreme events along a common direction, we can average them in order to extract a "typical" event. In order to do so, two points must be considered. First, the method used to reorient the events does not discriminate a direction. As a result, a naive average would lead the contributions from vortices rotating in opposite direction to cancel each other. Symmetrizing the fields such that all the vortices have a positive helicity at one given location near the center solves this problem. Also, our statistics might not be sufficient to converge to the average. Therefore, any interpretation regarding e.g. symmetry properties of the object must be done with caution. We have nevertheless checked that computing the same average for events coming for only half of the fields still gives the same results both qualitatively and quantitatively.

We compute the average of our 200 strongest events (for reproducibility, this corresponds to all events with a local Hölder exponent $h < 0.65$). We provide a visualization for this averaged event in figure 4 as well as in the Supplementary Materials for more details. The visualization includes the average of the local Hölder exponent h, the energy transfer D_I^ℓ and the energy dissipation D_ν^ℓ for the 200 events. Because they are not linear functions of the velocity field, they do not correspond to the values that would be computed from the averaged velocity.

The streamlines of the "typical" event match the pattern of roll vortices, with a change of helicity at the $x = 0$ plane, corresponding to the location of the minimum of Hölder exponent. This seems to be the typical behavior for extremely singular events. In particular, one might recognize in the streamlines the profile of a Burgers vortex (see

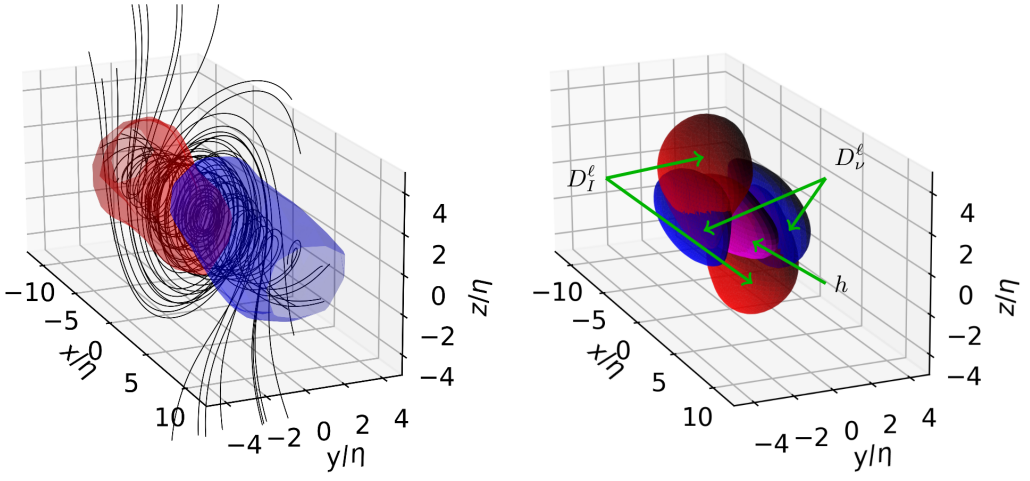

(a) (b)

FIGURE 4. (a): Streamlines of velocity. The axial velocity is oriented away from the $x = 0$ plane. The red (resp. blue) isosurface corresponds to an helicity of $H = 12$ (resp. $H = -12$). (b): The magenta isosurface corresponds to the local Hölder exponent $h = 0.75$. The red isosurface corresponds to $D_I^\ell = 60\epsilon$. The blue isosurface corresponds to $D_\nu^\ell = 40\epsilon$.

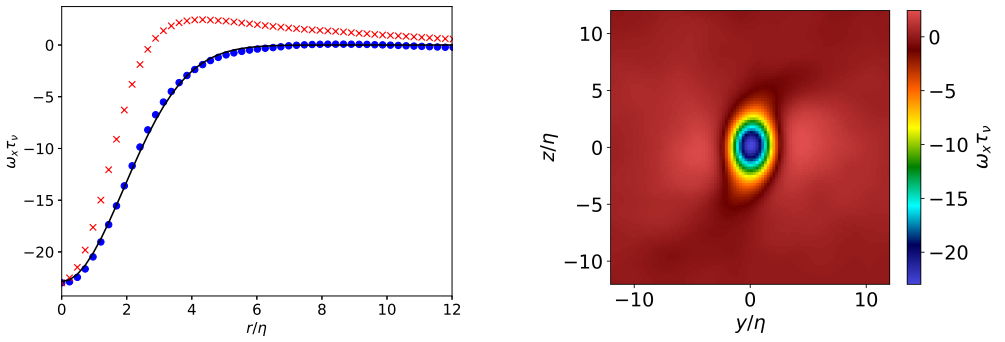

(a) (b)

FIGURE 5. (a) Fit of the component of the vorticity ω_x adimensionned by the Kolmogorov time scale τ_ν in the $x = 0$ plane for the averaged event. The vorticity along the z (resp. y) direction is represented with blue circles (resp. red crosses) while the Burgers fit is shown as a black continuous curve. (b) Colormap of $\omega_x\tau_\nu$ in the $x = 0$ plane for the averaged event.

Burgers 1948). An axisymmetrical Burgers vortex can be characterized by its vorticity profile:

$$\omega_x(r) = \frac{\Gamma}{2\pi\nu} \exp\left(-\frac{\sigma r^2}{2\nu}\right). \tag{3.4}$$

We can fit the profile of vorticity in the plane $x = 0$. This provides the values $\Gamma = -3.2$ and $\sigma = 1.2$. The fit works very well in the z direction but fails in the y direction, as illustrated in figure 5a. Note that the non axisymmetric Burger vortex would not provide a better result as the vorticity changes sign in the y direction. This asymmetry in the vorticity can be visualized in figure 5b.

We likewise observe a very strong non axisymmetry of the averaged D_I^ℓ and D_ν^ℓ. While the invariance by a rotation of π around the x-axis is a consequence of the orientation of the events before averaging, we do confirm the presence of structures of D_I^ℓ and D_ν^ℓ on both sides of the axis in individual events. A possible explanation to these non axisymmetric structures would be that extreme events correspond to an interaction between vortices of different strength, so that the weakest, least singular vortex is canceled out in the process of averaging. Furthermore, the reversal of helicity observed appears similar to what happens around a vortex reconnection (see Yao & Hussain 2020). In the sequel, we refine such hypothesis using time resolved data. Indeed, because of the way those events were extracted, it is not clear whether the snapshots captured are before, during or after the peak of the event.

3.4. *Link with the energy transfers*

While there are extreme events with negative energy transfer D_I^ℓ, i.e. energy going to the larger scales, this does not appear in the averaged event. This means that a typical extreme event transfer energy to smaller scales so that the average of the term D_I^ℓ stays positive around the region of low regularity.

We further observe that the energy transfer D_I^ℓ, and the dissipation energy transfer D_ν^ℓ, do not reach their maxima at the same location. Most of the energy transfer happens slightly earlier on the streamlines than the peak of dissipation. We currently do not have a physical explication for this phenomenon.

3.5. *Temporal evolution of an event.*

In order to maximize the number and intensity of events in the time resolved dataset, we choose the initial state of the simulation such that it will include a snapshot rich in extreme events from the Run II. Starting from the previous snapshot, we save a velocity field every 20 time steps (or about $0.2\tau_\nu$ where τ_ν is the Kolmogorov time). We collect this way 100 velocity fields 768^3 resolved in time.

From those, we detect 28 events that are below the threshold of $h = 0.7$ for more than 10 time steps. The strongest event actually reaches $h = 0.05$. We also extend the time window for a few selected events in order to try and observe their birth and decay. Movies of the corresponding time evolution can be found in the Supplemental Materials. For each events, we plot isosurfaces of vorticity (with red and blue coloring corresponding to positive and negative helicity respectively), local Hölder increments, energy transfers D_I^ℓ and dissipation D_ν^ℓ. We also plot the time evolution of the extrema for these quantities.

Those results appear to confirm the relation between extreme events of local Hölder exponent and vortex interaction. Indeed, most of the events observed are localized around two or more vortices. Moreover, we find several that are linked with vortex reconnection. One such event is represented figure 6. In this figure, we observe a peak of energy transfers and dissipation as the reconnection begins (figure 6d), followed by a drop of local Hölder exponent as it proceeds (figure 6f). It is however still unclear whether the irregular structure is caused by the reconnection itself or more generally by the interaction between the two resulting vortices.

In these events, extrema of D_I^ℓ, D_ν^ℓ and h are sometimes but not always concomitant. Figure 6 in particular shows that the peak of energy transfer to the lower scales occurs at the beginning of the reconnection (figure 6d), while the Hölder exponent has not yet dropped below 0.7. This chronology is reasonable as the building of irregular small scale structures detected using the local Hölder exponent requires some energy at the lower scales.

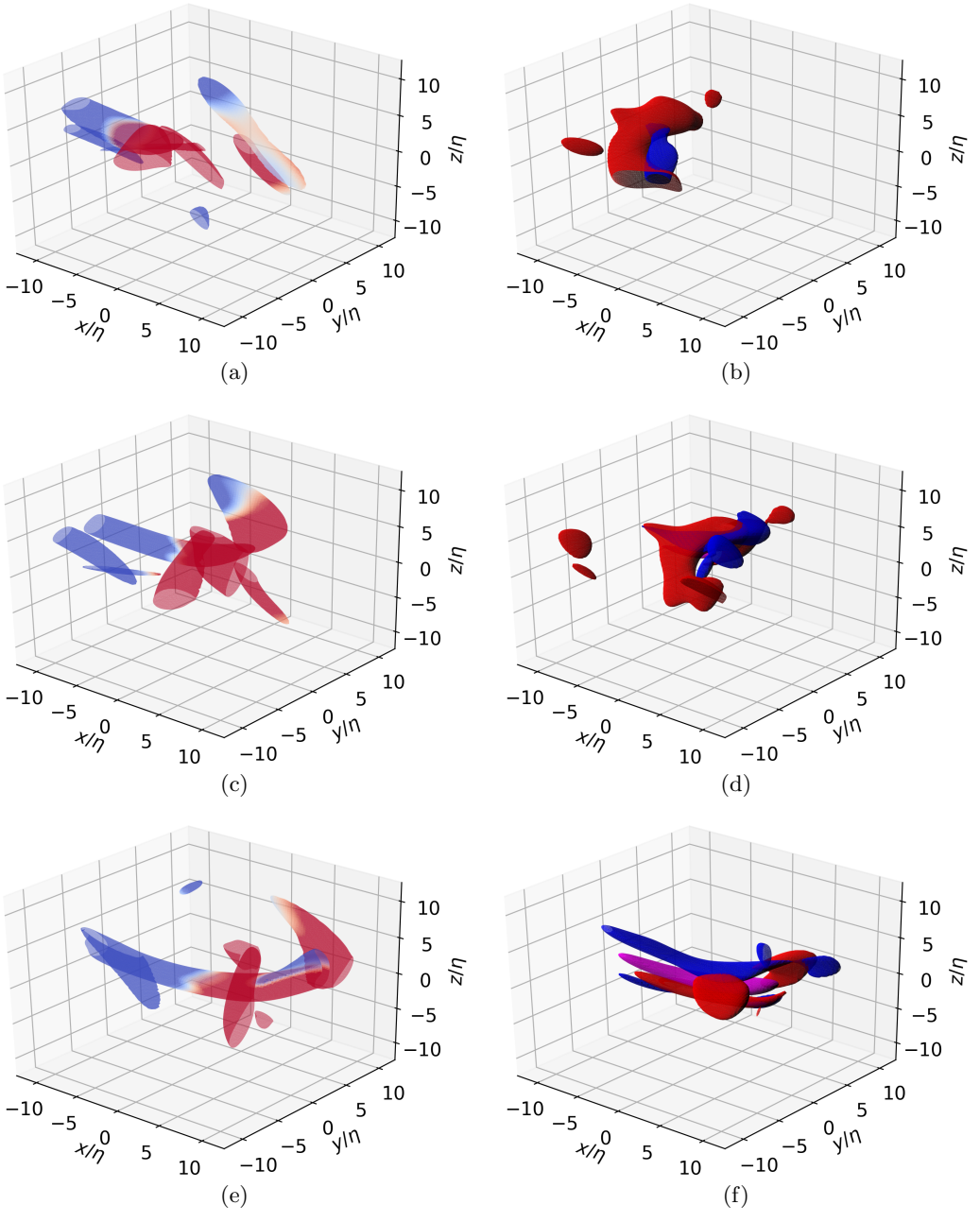

FIGURE 6. Snapshots of event 22: (a-b): Before the reconnection. (c-d): Beginning of reconnection. (e-f) Toward the end of reconnection. (a-c-e): Isosurfaces of vorticity $W = 60$ colored in red and blue respectively for positive and negative helicity. (b-d-f) Isosurface $h = 0.7$ in magenta, $D_I^\ell = 100\epsilon$ in red, $D_\nu^\ell = 5\epsilon$ in blue.

4. Discussion

In this paper, we have used the tool developed by Nguyen et al. (2019) to extract extremely singular events from numerical turbulent velocity fields. These events have been analyzed using local energy transfers at the Kolmogorov scale as well as the velocity

gradient tensor invariants. From these analysis, we derive several characteristics common to most singular events.

The first observation is that most events are "roll vortices", i.e. vortices with a change of helicity at the most singular point. The average structure computed from the 200 most singular events is similar to a Burgers vortex, with a weak non axisymmetry.

The second observation is that the local energy transfers around singular events are both away from the vortex axis and strongly non axisymmetric. The averaged event, as well as the individual events, exhibit two regions of energy transfer to lower scales D_I^ℓ located on both side of the main axis. The same observation can be done about the viscous energy dissipation D_ν^ℓ. To explain these facts, we emit the hypothesis that the extreme events are caused by interactions between at least two vortices, which would explain the non axisymmetry. This hypothesis is supported by the analysis of the time resolved data which shows that the singular events are associated with several vortices close to one another. Some cases involve a vortex reconnection, but we are unable to confirm the impact on the singularity of the event.

As those results are obtained from simulation data, all events detected are regularized at lower scale by the numerical scheme. In this case, the pseudo spectral method is filtering out wave numbers higher than k_{max}. As the small scales are expected to have a non negligible contribution for very singular events, using simulation data might have prevented us from observing more singular events. It would be interesting to reproduce this study using very well resolved experimental data, in order to validate the conclusions of the present work.

FN has been funded by École Normale Supérieure and was granted access to the HPC resources of IDRIS under the allocation A0062A01741 made by GENCI (Grand Équipement National de Calcul Intensif). This work was funded by the ANR EXPLOIT, grant agreement no. ANR-16-CE06-0006-01.

Declaration of Interests. The authors report no conflict of interest.

REFERENCES

Arneodo, A., Decoster, N. & Roux, S.G. 2000 A wavelet-based method for multifractal image analysis. I. Methodology and test applications on isotropic and anisotropic random rough surfaces. *The European Physical Journal B-Condensed Matter and Complex Systems* **15** (3), 567–600.

Batchelor, G. K. & Townsend, A. A. 1949 The nature of turbulent motion at large wave-numbers. *Proceedings of the Royal Society of London. Series A. Mathematical and Physical Sciences* **199** (1057), 238–255.

Burgers, J. M. 1948 A mathematical model illustrating the theory of turbulence. In Advances in applied mechanics, , vol. 1, pp. 171–199. Elsevier.

Debue, P., Valori, V., Cuvier, C., Daviaud, F., Foucaut, J.-M., Laval, J.-P., Wiertel-Casquet, C., Padilla, V. & Dubrulle, B. 2020 3D analysis of precursors to non-viscous dissipation in an experimental turbulent flow. *submitted to Journal of Fluid Mechanics* .

Dubrulle, B. 2019 Beyond Kolmogorov cascades. *Journal of Fluid Mechanics* **867**, P1.

Duchon, J. & Robert, R. 2000 Dissipation d'énergie pour des solutions faibles des équations d'Euler et Navier-Stokes incompressibles. *Séminaire Équations aux dérivées partielles* **2000**, 1–10.

Frisch, U. 1995 Turbulence: the legacy of AN Kolmogorov. Cambridge University Press.

Kestener, P. & Arneodo, A. 2004 Generalizing the wavelet-based multifractal formalism to random vector fields: application to three-dimensional turbulence velocity and vorticity data. *Physical Review Letters* **93** (4), 044501.

Kimura, Y. & Moffatt, H.K. 2014 Reconnection of skewed vortices. *Journal of Fluid Mechanics* **751**, 329–345.

Kolmogorov, A.N. 1941 The local structure of turbulence in incompressible viscous fluid for very large Reynolds numbers. *Dokl. Akad. Nauk SSSR* **30**, 9–13.

Kuzzay, D., Saw, E.-W., Martins, F., Faranda, D., Foucaut, J.-M., Daviaud, F. & Dubrulle, B. 2017 New method for detecting singularities in experimental incompressible flows. *Nonlinearity* **30** (6), 2381.

Leray, J. 1934 Sur le mouvement d'un liquide visqueux emplissant l'espace. *Acta Mathematica* **63** (1), 193–248.

Nguyen, F., Laval, J-P, Kestener, P., Cheskidov, A., Shvydkoy, R. & Dubrulle, B. 2019 Local estimates of Hölder exponents in turbulent vector fields. *Physical Review E* **99** (5), 053114.

Ooi, A., Martin, J., Soria, J. & Chong, M. S. 1999 A study of the evolution and characteristics of the invariants of the velocity-gradient tensor in isotropic turbulence. *Journal of Fluid Mechanics* **381**, 141–174.

Parisi, G. & Frisch, U. 1985 On the singularity structure of fully developed turbulence. *Turbulence and Predictability in Geophysical Fluid Dynamics and Climate Dynamics* .

Vincent, A. & Meneguzzi, M. 1994 The dynamics of vorticity tubes in homogeneous turbulence. *Journal of Fluid Mechanics* **258**, 245–254.

Yao, J. & Hussain, F. 2020 A physical model of turbulence cascade via vortex reconnection sequence and avalanche. *Journal of Fluid Mechanics* **883**, A51.